Available online at www.sciencedirect.com
SCIENCE DIRECT
Journal of Photochemistry and Photobiology A: Chemistry 176 (2005) 238–249
Journal of Photochemistry and Photobiology A:Chemistry
www.elsevier.com/locate/jphotochem

Deconstructing experimental rate constant measurements: Obtaining intrinsic reaction parameters, kinetic isotope effects, and tunneling coefficients from kinetic data for OH + methane, ethane and cyclohexane

Amy M. Sage, Neil M. Donahue *

Department of Chemistry and Chemical Engineering, Carnegie Mellon University, 5000 Forbes Avenue, Pittsburgh, PA 15213, USA

Abstract

Kinetic data for multiple OH–alkane reactions, including primary kinetic isotope data, can be fit simultaneously to extract constrained contributions from transition state vibrational activation, zero-point energy, and tunneling. We use data for single-pathway reactions: OH + methane, ethane, and cyclohexane, to obtain optimal 'intrinsic' parameters common to all reactions. This is possible because parameters specific to individual reactions, such as the pre-exponential term, can be accurately calculated with ease. Several intrinsic parameters – the barrier height, the tunneling temperature (imaginary frequency) and a transition state bending frequency (the radical attack angle) – scale together from reaction to reaction. This scaling is so precise that we can accurately fit data for OH + methane using intrinsic parameters derived for OH + ethane and OH + cyclohexane using only a single free parameter (the scaling factor). This strongly confirms our underlying hypothesis about the physics controlling the key transition state parameters and suggests that extrapolations in temperature and predictions for unmeasured reactions are potentially robust.

Keywords: Hydroxyl radical; Alkanes; Reactivity control; Kinetic isotope effects

1. Introduction

Reactions of alkanes and hydroxyl radicals (OH) initiate hydrocarbon oxidation sequences and constitute the dominant sink for OH in the atmosphere. These reactions are equally important in high-temperature combustion. Consequently, the extent and accuracy to which we know their rate constants limits the predictive abilities of chemical models. However, the myriad of hydrocarbons and broad temperature range relevant to these fields make the task of data collection daunting, highlighting the need for a theory of reactivity capable of predicting unknown rate constants. Furthermore, the H-atom transfers are among the most basic of reactions, so it is important to understand their dynamics in detail as part of a comprehensive theory of reactivity.

The connection between computational and experimental kinetics is a challenging one because the dynamics of even 'simple' reactions such as H-atom transfers are sufficiently interesting to obscure the relationship between the electronic potential energy surface (PES) and temperature-dependent rate constants. For reactions such as these, the region near a well-defined saddle point does indeed control the rate constant, and the energy of this saddle – the barrier height, E_b – does indeed play a vital role in the rate constant. There is also a well-defined pre-factor (related to the Arrhenius A factor) that we can calculate with great accuracy. However, at least three factors significantly influence the rate constant beyond the barrier height and pre-factor. First, zero-point energy changes, especially from vibrational modes both formed and lost in going from reactants to the transition state, augment the electronic energy. Second, vibrational excitation of key loose modes at the transition state greatly enhances the rate constant. This excitation corresponds to off-axis collisions by the attacking radical that nonetheless have sufficient energy to initiate the reaction, especially when the reaction channel is relatively 'wide'; it thus relates closely to the phase function of the cross-section for reactive scattering. Third, especially for H-atom reactions, tunneling can play a very significant role. This is most important at low temperature for reactions with relatively high and thin barriers.

* Corresponding author. Tel.: +1 412 268 4415.
E-mail address: nmd@andrew.cmu.edu (N.M. Donahue).

1010-6030/$ – see front matter © 2005 Elsevier B.V. All rights reserved.
doi:10.1016/j.jphotochem.2005.09.011

Computational reaction dynamics studies build up a rate constant, with either canonical, microcanonical, or trajectory calculations. They typically explicitly calculate each of these critical terms: the 'Born-Oppenheimer' surface of course, the zero-point correction, the phase function or the vibrational partition function at the transition state, and a tunneling or quantum transmission coefficient. The combined terms are then compared with experimental data, though in very, very few cases has this been accomplished successfully without at least some parameter tuning. Because they are time intensive, these studies almost invariably focus on a single-reaction.

It is tempting to ask whether experimental data can be mined to constrain some or all of these terms accurately. This turns out to be nearly impossible for a single-reaction, but by analyzing multiple reactions within a unified theoretical framework, it is possible to invert data to discover the contributions of these terms to multiple reactions. For this purpose, we have developed a method for determining computationally relevant parameters from experimental data. The method simultaneously fits sets of data for the reactions of OH with a homologous series of standard and deuterated alkanes, allowing the variations within and among datasets to constrain fundamental physical parameters that are generally inaccessible using single-reaction kinetics studies. Using this method, we are able to abstract parameters such as the Born-Oppenheimer barrier height and the transition state vibrational frequencies, which are characteristic not just of an individual reaction, but of the entire reaction series, from the available experimental data. The method is tied to the fundamental chemical physics controlling rate constants and consequently demonstrates considerable skill in extrapolation — both extending beyond the range of individual measured rate constants and predicting the behavior of additional reactions with a single scaling parameter.

2. Methods

2.1. Background

Our objective is to develop a function to fit kinetic data that can describe an individual rate constant over the full temperature range, from combustion temperatures to 100 K and below, while also describing the kinetic isotope effects. On top of this, we wish to describe and understand the evolution of the rate constant through a homologous series of reactions, so the function should be able to describe this evolution with the minimum necessary physics. Ultimately, this serves a practical and a fundamental purpose. The practical purpose is to accurately extrapolate rate constants well beyond the experimental temperature range and also to accurately predict branching ratios in reactions with multiple pathways where branching data are unavailable. The fundamental purpose is to study the chemical physics that controls the properties critical to determining rate constants and to test a specific hypothesis of how that physics evolves in homologous reaction sequences.

That hypothesis is that the Born-Oppenheimer barrier height (the electronic potential energy of the transition state relative to the electronic potential energy of the reactants), the barrier width (defined by the imaginary frequency, expressed as a tunneling temperature), and two nearly degenerate transition state bending modes (corresponding to the collision angle of the radical relative to the C–H bond axis), all evolve in a highly correlated manner, with the barrier height, tunneling temperature, and bending frequency declining together as the curve-crossing energy defining the transition state drops from one reaction to the next.

Our basic function is based on transition state theory, including tunneling. The starting point is a functional form presented in several papers over the last decade [1]. Our early work explored the physics controlling the curve-crossing itself, establishing that changes in the curve-crossing energy were driven almost entirely by changes in an ionic-excited state defined by a single electron transfer from the donor hydrocarbon to the acceptor radical (with initial energy IP-EA) [2]. We confirmed the basic validity of our central hypothesis for atom–alkane reactions in a subsequent paper [3], considering only reactions with a single-reaction pathway to simplify the analysis. Here we extend this treatment to OH–alkane reactions, which forces treatment of a more complicated transition state because of the added modes related to the linear radical, but which also provides a richer data set including high-quality primary kinetic isotope data for fully deuterated alkanes. As before, we focus our attention on reactions with a single-pathway — specifically OH + methane, ethane, and cyclohexane.

The function focuses on key modes undergoing a substantial transformation as the system moves from reactants to the transition state — for example, reactant translation orthogonal to the reaction coordinate becomes rotation at the transition state, and the rotations of the individual reactants become bending vibrational modes. The reactants have six translational and five rotational degrees of freedom, while the transition state has three of each; therefore, five internal modes of the transition state correspond to external modes of the reactants. Those five modes dominate the rate constant, and they are depicted in Fig. 1. Only one of these modes is relatively simple to treat — the internal rotation of the O–H directly corresponds to one of the OH external rotations. This leaves four internal transition state modes crucial to determining the rate constant.

Energies important to the transition state are shown in Fig. 2. In this paper we shall describe energies in Kelvin, so for the sake of consistency we will use characteristic temperatures $\theta = E/R$, though we shall discuss frequencies in wave numbers, with $\theta_\nu = 1.44\nu$. The important energies include the electronic energy of the reactants (which is the reference), the zero-point energy lost from the reactants at the transition state ($\delta\nu$, presumably mostly the lost C–H stretch in the alkane, which is the reaction coordinate at the transition state), the zero-point energy gained from the four transition state vibrations discussed above, and a van der Waal's energy, θ_v, which serves as a reference energy for the barrier $\theta_0 = \theta_b - \theta_v$ and is important when various terms are scaled for different reactions. These are joined by the imaginary frequency of the reaction coordinate itself, which we depict as a characteristic tunneling temperature (θ_t, see below). The adiabatic transition state critical energy θ_{crit} is the zero-point

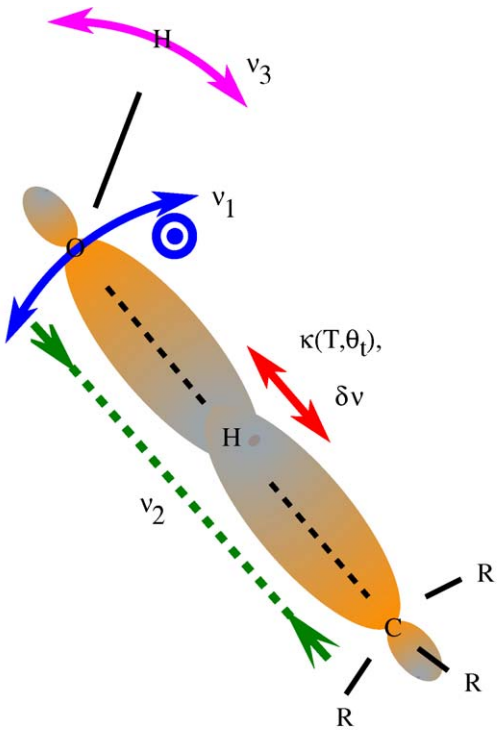

Fig. 1. Modes associated with OH attack on an alkane, with the simplifying assumption of a linear O—H—C structure. Translation of the OH radical becomes two quasi-degenerate O—H—C bends (ν_1) and one O—H—C stretch (ν_2, which is the reaction coordinate far from the TS geometry). Rotation of the OH becomes an H—O—H bend (ν_3) as well as an internal rotation about the O—H—C bond. Other crucial factors to the transition state are also shown, including the tunneling (κ), which is controlled by an imaginary frequency here expressed as a tunneling temperature (θ_t, see text) as well as lost zero-point energy associated with the C—H stretch (δ_ν).

corrected electronic energy $\theta_0 + \Delta\theta_{zp}$, where $\Delta\theta_{zp} = (1/2)\ 1.44\ (2\nu_1 + \nu_2 + \nu_3 - \delta\nu)$.

Almost all of the other vibrational modes of the reactants have a minimal influence — their only significant role, if they have one, is to change the overall zero-point energy of the system. The exceptions are very loose modes, torsions and backbone undulations that may change frequency at the transition state; for the most part these modes influence the preexponential in proportion to the fractional change in frequency ($Q^{TS}_{vib}/Q^{R}_{vib} \simeq \nu_{TS}/\nu_R$). For this reason, we treat these modes as causing a constant contribution to the rate constant and include them with the other parts of the constant pre-factor.

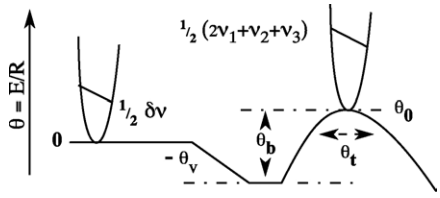

Fig. 2. Energies important to the transition state (in Kelvin). The critical energy (θ_0) is the sum of a barrier term (θ_b) and a van der Waal's term ($-\theta_v$). Tunneling depends on a tunneling temperature θ_t, related to the imaginary frequency. Zero-point energy is subtracted by modes lost from the alkane ($\delta\nu$) and gained at the transition state ν_1, ν_2, ν_3, also depicted in Fig. 1.

2.2. The single-reaction function

The canonical transition state theory (TST) rate constant, corrected for tunneling, is

$$k = n_H \kappa(1/T, \theta_t) \frac{k_B T}{h} \frac{Q^{TS\neq}}{Q^{react}} \exp(-(\theta_0 + \Delta\theta_{zp})1/T) \quad (1)$$

where n_H is the number of equivalent hydrogens in the alkane, k, the tunneling correction, and $k_B T/h$ is the residual partition function for the reaction coordinate. Following standard practice, we break the partition functions for the transition state ($Q^{TS\neq}$) and the reactants (Q^{react}) into terms for different modes of motion: $Q = Q_{elec} Q_{trans} Q_{rot} Q_{ir} Q_{vib}$, where 'ir' connotes internal rotors. Because of the ratio in Eq. (1), only modes that change significantly from the reactants to the transition state contribute significantly to the rate constant. Furthermore, the translational, and rotational parts of the expression are extremely well known — even a crude estimate of the transition state geometry will give accurate moments of inertia. The electronic term for the reactants (the OH radical) is also well known, and we shall assume that the transition state electronic degeneracy is simply 2. Taking the log of Eq. (1) and grouping the terms, we arrive at our basic equation for the rate constant:

$$\ln k = \ln n_H + \ln \kappa + \ln Q_{vib} + \ln g_{elec} + \ln B + \ln(1/T) - ((\theta_0 + \Delta\theta_{zp})1/T) \quad (2)$$

The overall temperature dependence (specifically the $\ln 1/T$ term), results from the net effect of six translational modes becoming three translational modes and five external rotations becoming three external and one internal rotations at the transition state — the pre-factor ($\ln B$) in Eq. (2) is independent of temperature.

For the purposes of fitting and interpretation, it turns out to be expedient to separate Eq. (2) the following way:

$$\ln k = [\ln \kappa] + [\ln Q_{vib}] - [\Delta\theta_{zp}/T] + [\ln n_H + \ln g_{elec} + \ln B + \ln(1/T) - \theta_0/T] \quad (3)$$

We shall consider each of the bracketed terms in turn, working from right to left: first is the 'Born-Oppenheimer' term:

$$[\ln n_H + \ln g_{elec} + \ln B + \ln(1/T) - \theta_0/T]$$

It contains numerous parts but only one real unknown — the barrier, θ_0, itself. We use the number of equivalent hydrogens, n_H instead of a rotational symmetry number as this will make later treatment of substituted alkanes and their isotopomers far simpler. The electronic partition function, g_{elec}, combines an assumed transition state degeneracy of two with a spin–orbit splitting for $^2\Pi_{1/2} \leftarrow {}^2\Pi_{3/2}$ of 126.23 cm^{-1} [4] for an overall ratio:

$$\ln g_{elec} = -\ln[2 + \exp(-1.44(126.23/T))] \quad (4)$$

With the negative sign showing that the net effect is to reduce the rate constant. The 'pre-factor', $\ln B$ arises from the external modes, the internal OH rotation at the transition state, and any

loose vibrations whose frequencies change enough to contribute:

$$\ln B \simeq \ln\left[10^{-9}\mu^{-3/2}\sqrt{\frac{I_{\mathrm{IR}}I_{\mathrm{TS}}^3}{I_{\mathrm{OH}}^2 I_{\mathrm{mol}}^3}}\frac{Q_{\mathrm{vib}}^{\mathrm{TS}}}{Q_{\mathrm{vib}}^{\mathrm{react}}}\right] \quad (5)$$

where μ is the collisional reduced mass, in amu, I_{TS}^3 and I_{mol}^3, the products of three moments of inertia for the transition state and the alkane, I_{OH}^2, the moment for the linear OH rotation and I_{IR} is the (nearly identical) moment for the internal OH rotation, all in amu-Å^2. Finally, $Q_{\mathrm{vib}}^{\mathrm{TS}}/Q_{\mathrm{vib}}^{\mathrm{react}}$ accommodates any vibrations shared by the reagents and transition state that may be sufficiently loose and different to have a ratio different from unity (backbone bends and torsional modes). The residual temperature dependence is $1/T$, which yields the overall behavior shown.

One of the keys to our fitting approach is that this complete $\ln B$ term can be tightly constrained with minimal effort, using low-level ab initio or semi-empirical transition state structures or even an educated guess. In our case we use a combination of high-level structures from the literature [5,6], and structures found using either Hartree-Fock or density functional calculations, keeping to a single level of theory for a single-reaction to ensure that errors cancel. In practice, the residual contributions of loose backbone modes for reactions like OH + cyclohexane are the leading sources of error in $\ln B$, and that error is small.

The next two bracketed terms in Eq. (3) are fairly straightforward. First we have the zero-point energy term, $[\Delta\theta_{\mathrm{zp}}/T]$, which includes contributions from the vibrations already discussed. We separate this from the 'Born-Oppenheimer' term because changes to the zero-point energy term are a major contributor to the primary kinetic isotope effect. Next is the vibrational contribution due to the 'new' transition state modes, ν_1, ν_2 and ν_3, giving

$$\ln Q_{\mathrm{vib}} = -[2\ln(1-\exp(1.44\nu_1/T)) + \ln(1-\exp(1.44\nu_2/T)) + \ln(1-\exp(1.44\nu_3/T))] \quad (6)$$

In practice, only the contribution from ν_1 is interesting — the frequency is low and it varies from reaction to reaction; while this mode is obviously not degenerate in the real reaction, treating it as quasi-degenerate with a single frequency significantly simplifies the fitting and, as we shall show, it works well. The two other frequencies are high (at 740 and 1000 cm^{-1}), as we shall discuss below. When the temperature is equal to the frequency of a vibration the partition function is only 1.3, meaning that the rate constant is increased by 30% due to activation of this mode; consequently, the stiff modes ν_2 and ν_3 contribute only modestly to the overall vibrational partition function even at the highest temperatures. However, the zero-point energy of these stiff modes is substantial.

The tunneling coefficient, κ, is based on Truhlar's one dimensional function [7]:

$$\kappa = \begin{cases} \dfrac{\theta_{\mathrm{t}}/T}{\theta_{\mathrm{t}}/T-1}\left(\exp\left[\left(\dfrac{\theta_{\mathrm{t}}}{T}-1\right)\dfrac{\theta_{\mathrm{crit}}}{\theta_{\mathrm{t}}}\right]-1\right) & T\le\theta_{\mathrm{t}} \\ \dfrac{\pi\theta_{\mathrm{t}}/T}{\sin(\pi\theta_{\mathrm{t}}/T)} - \dfrac{\theta_{\mathrm{t}}/T}{1-\theta_{\mathrm{t}}/T}\exp\left[\left(\dfrac{\theta_{\mathrm{t}}}{T}-1\right)\dfrac{\theta_{\mathrm{crit}}}{\theta_{\mathrm{t}}}\right] & T>\theta_{\mathrm{t}} \end{cases} \quad (7)$$

A point to emphasize is that tunneling occurs through the zero-point corrected barrier (θ_{crit}). While the tunneling temperature can be related to the imaginary frequency: $\theta_{\mathrm{t}} = \hbar\omega_i/(2\pi k_{\mathrm{B}})$, we regard this function as a parameterization for the far more complicated dynamics of tunneling and thus do not expect that computational imaginary frequencies will be appropriate. The tunneling temperature is simply the temperature *below* which $\kappa \gg 1$ — for example for $T = \theta_{\mathrm{t}} = 100$ K and $\theta_{\mathrm{crit}} = 1000$ K, $\kappa \simeq 10$. Using multiple datasets, including primary kinetic isotope effects, we propose to constrain the tunneling coefficient using κ and θ_{t} as the function and adjustable parameter with the appropriate characteristics.

At this point, there are seven 'free' parameters associated with Eq. (3): $\{\ln B,\ \theta_{\mathrm{b}},\ \theta_{\mathrm{t}},\ \nu_1,\ \nu_2,\ \nu_3,\ \delta\nu\}$. These parameters can be used to fit rate constant data for a single-reaction with a single reactive pathway, provided that some a-priori constraints can be applied to condition the fit. In this case, we expect the a-posteriori parameters and uncertainties to relate to the chemical physics responsible for them, described above.

2.3. Kinetic isotope effect

Our ultimate objective is not to describe a single-reaction but a succession of them. Specifically, we want to treat the primary kinetic isotope effect (pKIE) due to deuteration as well as the evolution of both the protonated and deuterated rate constants from one reaction to the next in a homologous series. The pKIE is relatively straightforward. Deuteration lowers the tunneling temperature by lowering the imaginary frequency, and it also lowers the frequency loss $\delta\nu$. In both cases we expect the effect to scale with the square root of the ratio of reduced masses in the protonated and deuterated systems for the important modes, which we will call μ, i.e. $\theta_{\mathrm{t}}^{\mathrm{D}} = \theta_{\mathrm{t}}^{\mathrm{H}}/\sqrt{\mu}$. We assume that the reduced mass for tunneling and the vibrational change are the same, and that the ratio is approximately 2. In addition to this effect, there is a small change in the pre-factor, $\delta\ln B$, for the deuterated system $\ln B^{\mathrm{D}} = \ln B^{\mathrm{H}} - \delta\ln B$. The deuterated systems collide somewhat more slowly because of the larger reduced mass and smaller change in moments of inertia. This can be calculated to higher accuracy than even $\ln B$ itself.

2.4. Homologous series

The evolution in a homologous series is more interesting. A crucial theoretical finding is that the three most important parameters in Eq. (3) – θ_{b}, θ_{t}, and ν_1 – are highly correlated. In particular, the physics that drives variations in the barrier height simultaneously drive variations in the imaginary frequency (and thus θ_{t}) and in the TS bending frequency (ν_1). As the barrier lowers from one reaction to the next, the reaction channel gets wider and the barrier gets relatively broader. This is because these terms all arise from the same frontier–orbital interactions; the bending, for example, is defined by a quadratic energy rise from the transition state minimum as frontier orbital overlap decreases away from the optimal orientation. The absolute curvature is thus a dimensionless overlap term scaled by the crossing energy; as the crossing height drops, so does the bending frequency.

This is responsible for the emergence of "stripping" behavior seen in low barrier reactions, such as Cl + ethane. It is also why there is usually a tight relationship between barriers and A-factors; this is discussed in detail in our earlier work [3,1].

The theoretically derived correlations among the parameters permit well-constrained fitting of rate data to functions of this form. This in turn provides a much tighter link between rate data and theoretically derived barriers. In particular, the θ_b parameter obtained from a fit using Eq. (3) is closely related to a Born-Oppenheimer barrier, whereas the E_a obtained from a log-linear Arrhenius fit is not. From the perspective of fitting rate constant data, this means that as we move from one reaction to the next, we expect the three parameters to scale together, following a single scaling parameter s_n for reaction n. As it turns out, the data reveal a slightly more complicated relationship — the apparent barrier changes more rapidly than either ν_1 or θ_t. A fully consistent interpretation is that the reference energy for the curve-crossing physics is lower than the reactant energy by an amount we refer to as θ_v, shown in Fig. 2 (a van der Waal's energy).

$$\theta_0 = \theta_b + \theta_v$$

With that addition, relative to a reference reaction, 1, the correlated parameters for a second reaction n are

$$\theta_{b,n} = s_n \theta_{b,1} \tag{8}$$

$$\theta_{t,n} = s_n \theta_{t,1} \tag{9}$$

and

$$\nu_{1,n} = s_n \nu_{1,1} \tag{10}$$

2.5. Fit interpretation

In this model, we consider the rate constants for reactions in a homologous series to be governed by a set of intrinsic parameters common to all of the reactions: $\{\theta_v, s_n\theta_b, s_n\theta_t, s_n\nu_1, \nu_2, \nu_3, \delta\nu, \mu\}$, and a smaller set of parameters specific to each reaction n: $\{s_n, n_H, \ln B, \delta \ln B\}$. The specific parameters other than s_n are more or less exactly known — we shall fit them without allowing any significant variation. The scaling parameter s_n itself is perhaps the most fundamental; we expect it to vary with the excited state energies driving the curve-crossing energy (e.g. IP-EA). Some of the intrinsic parameters are less well known, while others we can constrain; for instance we expect that $\mu = 2$ and will fit data with this constraint, and computations show $\nu_2 \simeq 760\,\mathrm{cm}^{-1}$ and $\nu_3 \simeq 1000\,\mathrm{cm}^{-1}$, which we will constrain as well (though not absolutely).

The rest of the parameters are constrained by multiple data sets. The relationships are shown in Fig. 3, which shows the stylized contributions of these various parameters to two reactions (in the top panels) and their primary kinetic isotope effects (in the bottom panels). We plot 'rate constants' due to the bracketed terms in Eq. (3). The black line is the 'Born-Oppenheimer' rate constant, including the electronic partition function, as discussed. The blue line adds the zero-point energy correction, while the green line adds the vibrational partition function, and finally the red line adds the tunneling correction. On the lower panels, the black line shows the pKIE due to changes in the pre-factor ($\delta \ln B$), the blue line shows changes due to zero-point energy changes $\delta\nu$, and the red line shows changes due to tunneling $\Delta\theta_t$. The left-hand reaction is slow, with a large scaling factor s, while the right-hand reaction is fast, with a small scaling factor.

For the top panels in Fig. 3 we have idealized the form of the 'Born-Oppenheimer' rate constant, neglecting curvature driven by either the $\ln 1/T$ term or the electronic partition function. The constraints begin at the intercept of the black and blue lines, which is determined by $\ln B$. High-temperature rate constants far above this value rely almost exclusively on Q_{vib}, which is dominated by frequencies well to the right of a given temperature (for example, in the first panel ν_1 is shown at 250 K, so it dominates Q_{vib} below at least 1000 K). The fundamental slopes are governed by the barrier height as well as the zero-point energy. At relatively low temperatures, tunneling can increase the rate constant, as shown. Moving from a slow reaction to a fast one (left to right panels), the simultaneous lowering of the barrier, bending frequency (ν_1) and tunneling temperature will lower the apparent slope (the activation energy), significantly increase the offset between the observed rate constants and $\ln B$ at high-temperature, and sharply reduce the tunneling (note that the ν_1 and θ_t indicators move to the right in the second panel).

In our model, the pKIE has only three contributing factors. The pre-factor change $\delta \ln B$ provides a constant offset at all temperatures. The zero-point energy change is due solely to the change in $\delta\nu$: $\Delta\delta\nu = \delta\nu\,(1 - 1/\sqrt{\mu})$. We expect this factor to generate a pKIE that increases toward low temperature in a linear fashion, as shown. This contribution is identical across the homologous series of reactions. Finally, the tunneling contribution will generate a non-linear increase toward low temperature, with the magnitude changing dramatically across the series of reactions. Because our model contains only these three contributions to the pKIE, the inversion (the fit) will apportion contributions to each term; as such it cannot prove that these three terms alone dominate the pKIE but it can demonstrate consistency. One possible influence we neglect is any variation in the new transition state frequencies (ν_1, ν_2, ν_3) upon deuteration — while we do not expect this to be large, in some cases the contribution of Q_{vib} to the overall rate constant in Eq. (3) is so substantial that even a small change in Q_{vib} could influence the pKIE.

While our overall functional form has quite a few parameters, they are all either tightly constrained a-priori or forced into an intricate relationship by the data. Consequently, we expect that success in treating multiple reactions within this framework will strongly test and confirm our underlying hypothesis.

2.6. Fitting specifics

Our actual fitting procedure is to code the functions above and to carry out standard non-linear least-square optimization with constrained parameters, as described in an earlier publication [8]. The significant detail is that we provide both a-priori parameters (the guess) and a-priori parameter uncertainties (the constraint). These parameters are treated as normal constraints, meaning that the objective function is penalized in proportion

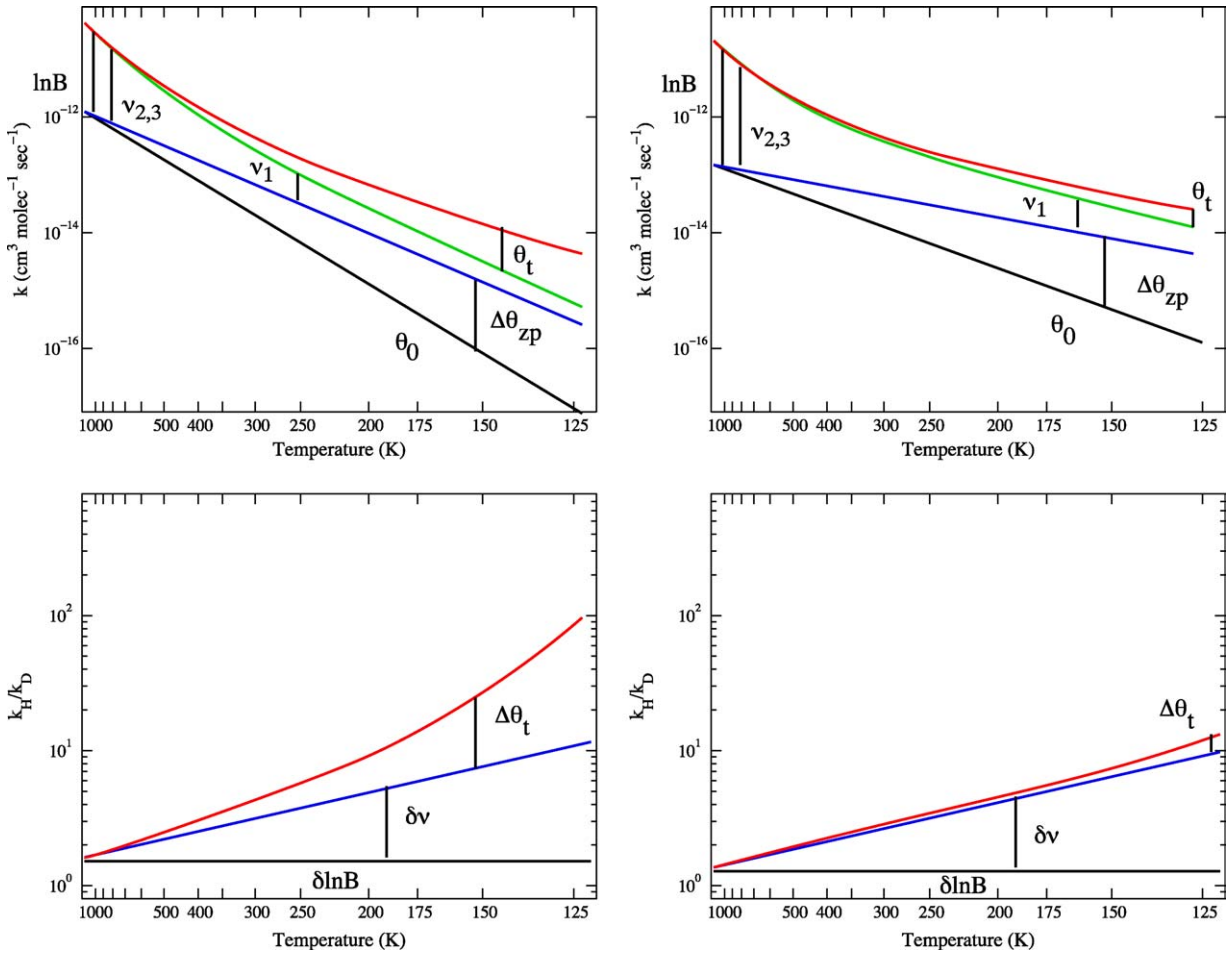

Fig. 3. Interpretation of fit parameters (see text for the relevant functions) for two reactions, one slow (to the left) and one fast (to the right). The parameters significant to different terms are shown on the figures, with placement indicating the rough temperature ranges where each parameter is most tightly constrained — for example the pre-factor ($\ln B$) constrains the intercept. The top panels show the rate constant. The 'Born-Oppenheimer' rate constant, including the electronic potential energy surface and the electronic degeneracy of the reactants and transition state, is shown in black. The zero-point corrected rate constant (assuming a net decrease in the effective barrier) is shown in blue. The contribution from active transition state vibrations is shown in green, while the contribution from tunneling is shown in red. The lower panels show the kinetic isotope effect. The effect of pre-factor changes is shown in black. The effect of zero-point energy changes in shown in blue. The effect of changes to the tunneling coefficient is shown in red. Slow reactions with a high barrier (and light reagents) have a relatively large pre-factor but a strong temperature dependence. The transition state vibration is stiff (ν_1 at 250 K) and tunneling is important (θ_t at 150 K). Fast reactions with a low barrier (and heavier reagents) have a relatively small pre-factor but a slight temperature dependence. The transition state vibration is loose (ν_1 at 175 K) and tunneling is negligible (θ_t at 125 K and a low barrier). The kinetic isotope effect due to zero-point changes is identical in each case, but tunneling is far more important in the slow reaction.

to the square of the number of standard deviations away from the a-priori guess that the ultimate parameter estimate lies. For instance, for a well-known parameter such as $\ln B$, we might provide an a-priori estimate of -22.25 ± 0.02, and the a-posteriori estimate will be unlikely to deviate much more than 0.02 from that guess, unless the data are grossly inconsistent with that constraint.

The constraints can play two roles. The first is that we really do have good a-priori information on the parameter value — $\{\ln B, \delta \ln B, n_H\}$ fall into this category. The second is simply to condition the fit. For example, we shall include all of the 'intrinsic' parameters defined above in even our single-reaction fits, but in this case the van der Waal's term θ_v and the barrier term θ_b are degenerate, so one term — θ_v, must be specified arbitrarily (or, in fact, based on subsequent determination of the best value). Some parameters fall in the middle — for example we regard ab initio determinations of ν_2 and ν_3 as only semi quantitative, but the data do not constrain them significantly. Consequently, we can provide a looser a-priori constraint — for example 760 ± 20 for ν_2.

3. Results

Selected subsets of the available literature data for the reactions of OH with methane [9–13], ethane [14–19,2,20–22], and cyclohexane [23,19,14] and their perdeuterated analogs [10,11,14] were fit, both individually and simultaneously, to the function given in Eq. (3). Because we are interested in both absolute and relative values of rate constants (both the pKIE and the differences between different reactions are relative phenomena), we must be very careful to consider the absolute accuracy of the individual data from each publication. It is safest to consider high-quality data from a single laboratory; for example, kinetic isotope studies from the Tully laboratory form the foundation

for this work. However, we propose to use the wider literature to greatly extend the temperature range of individual datasets, and so we must go beyond individual laboratories.

We can include individual calibration factors with each data set, in essence fitting for the systematic errors in each experiment [8]; however, to include these parameters in the already extensive fitting exercise described above would be overwhelming. Instead, we have selected literature data which show strong overall agreement when we fit the individual reactions including a calibration factor (error factors less than 5%); visually, this can be verified by the absence of any systematic offsets between different data sets over a common temperature range. The sole exception to this is data from an extremely low temperature study of OH + ethane using the CRESU Lavalle nozzle experiment [20]. These data extend the range of the OH + ethane data to 140 K, but over the range where they overlap with multiple other data for the reaction they are systematically 18% higher than the other data. Consequently, we multiply all rate constants from this study by 0.85 before plotting and analysis. Another example of this offset appears to be the recent results for OH + methane at high-temperature [24]. Visual inspection reveals that these data appear to fall systematically lower than other literature data by a factor of approximately 0.7. While we could 'calibrate' these data with a factor of 1.4 and include them, the overlap with existing data is not large and the temperature range includes substantial activation of the tight modes ν_2 and ν_3, which are not well constrained by any other data in our combined data set. Thus, while we plot these high-temperature OH + methane data, we do not include them in our fits.

3.1. A-priori constraints

One of the most important aspects of this method is to develop strong a-priori constraints on the pre-factor, $\ln B$. Fortunately, this is easy. In each case we use the highest-level theoretical geometries available that consistently treat the reactant and transition state structures. For methane and ethane these are computational results from the Melissas and Truhlar [6,5]. For cyclohexane, on the other hand, we use a simplified approach, finding a transition state geometry for the H + chyclohexane reaction at a low-level of theory (UHF/STO-3G) and simply replacing the attacking H-atom with a mass of 17 in the frequency calculation.

3.2. Fitting results

The individual fits have loose a-priori constraints on all parameters except $\ln B$ and thus represent our best estimate of the 'true' experimental values, interpolated to any temperature between the limiting temperatures of each data set. The fidelity of any extrapolation is an interesting issue discussed below. The results of these individual least-square fits to each of the six-reaction datasets are shown as lines in Fig. 4, along with the results of the simultaneous fits of two, four and all six reaction, indicated by the terminal markers at high and low temperature. Additional data (not included in the fits) are also shown for reference [24,25].

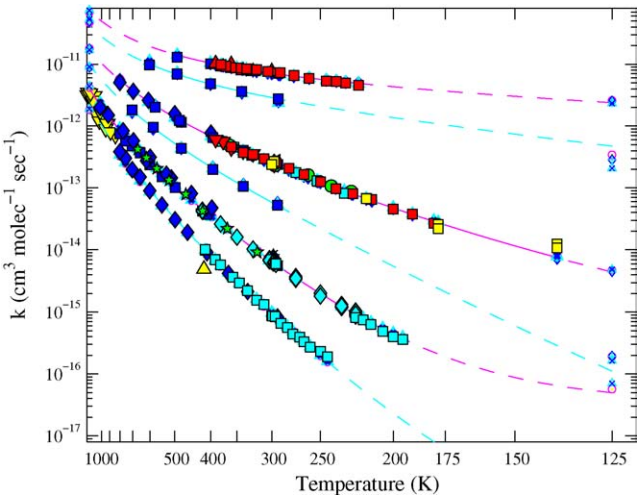

Fig. 4. Data and fit results in an Arrhenius plot for OH + methane, ethane, and cyclohexane (fully protonated and deuterated; OH + methane-D_4 is at the bottom, OH + cyclohexane-H_{12} is at the top). Magenta lines mark the protonated data, while cyan lines mark the deuterated data. Individual fits are discussed in the text; solid lines indicate the range of data used in the fits, while dashed lines are extrapolations to the indicated temperature limits. Symbols at the limits show fit results for various functions combining the datasets, including kinetic isotope effect (pKIE) fits for individual reactions (yellow in magenta) and multiple reaction pKIE fits (blue and cyan).

The six-reaction simultaneous fit produced the parameters listed in Table 1. These parameters were optimized from a-priori guesses based on low-level calculations and the individual reaction fits. Parameters were more or less constrained in accordance with our confidence in these guesses. For example, values of the pre-factor terms, $\ln B$, for each reaction were calculated from transition state theory and constrained to within less than 1% of the calculated value, while the desired results of the fit, such as the terms representing the barrier energy and tunneling temperature, were constrained only to within 10% of their a-priori values (and indeed θ_b was left completely unconstrained in the individual fits).

Ethane was used as the reference reaction for the scaling parameter s_n. Relative to ethane, the set of intrinsic parameters common to all three reaction systems was scaled by 1.73 ± 0.02 for methane and by 0.46 ± 0.01 for cyclohexane. Using this scaling factor, the six-reaction fit agrees with the included experimental data with high fidelity over the entire available data range, with the vast majority of the data lying within a few percent of the fit.

Extrapolation of the best-fit lines to the individual dataset and of the six-reaction fit to temperatures well below the experimental range leads, at worst, to a difference of less than a factor of two in the predicted rate constant for cyclohexane-d12 + OH at 125 K. Most of the extrapolations shown in Fig. 4 fall within 30% of each other for a given reaction.

3.3. Contributions to the rate constants

According to our model, as expressed in Eq. (3), the rate constant for a reaction is the sum of four contributing terms: a Born-Oppenheimer barrier energy term, the zero-point energy

Table 1
Parameters from the six-reaction fit

	Intrinsic parameters	
Θ_v	Van der Waal's energy (K)	-848 ± 70
Θ_b	Born-Oppenheimer barrier (K)	1446 ± 52
Θ_t	Tunneling temperature (K)	101 ± 2
ν_1	Two degenerate O—H—C bends (cm^{-1})	120 ± 2
ν_2	O—H—C stretch (cm^{-1})	767
ν_3	H—O—H bend (cm^{-1})	986
$\delta\nu$	Change in zero-point energy (cm^{-1})	1331 ± 63
μ	Ratio of reduced mass (μ_D/μ_H)	2

	Compound-specific parameters	Methane	Ethane	*c*-hexane
s_n	Scaling factor	1.75 ± 0.03	1	0.45 ± 0.01
n_H	Number of equivalent hydrogens	4	6	12
$\ln B$	Pre-factor	−21.41	−22.47	−23.96
$\delta \ln B$	Change in pre-factor (H—D)	−0.60	0.45	−0.09

The parameters intrinsic to all six-reaction are shown in the upper panel, and reaction-specific parameters are given in the lower panel. Values without uncertainties were tightly constrained.

correction, the vibrational partition functions of the three reaction modes, and a tunneling term. The contributions of each of these terms to the overall rate constants as determined by the six-reaction fit are shown in Fig. 5, which follows the scheme depicted in Fig. 3. The most obvious difference between that idealized presentation and the actual fit results is that the net effect of the zero-point energy changes is to increase the barrier height, meaning that the added zero-point energy from ν_1, ν_2, and ν_3 outweighs the zero-point energy lost to the reaction coordinate, $\delta\nu$. The result is that the vibrationally adiabatic rate constant (shown in blue) lies below the 'Born-Oppenheimer' rate constant (shown in black). This is something of a surprise, and we shall discuss it in more detail below. The difference between the reaction rate due to the vibrationally adiabatic barrier and the observed reaction rate (shown in red) is jointly attributable to the vibrational and tunneling terms. At high-temperature, the vibrational term (shown in green) progressively increases from methane to cyclohexane, nicely compensating for the increasing difference between the observed reaction rate and that calculated due to the relatively constant potential energy surface barrier. At low temperatures, the tunneling term decreases along the same series as tunneling becomes progressively less significant with increasing molecular size; qualitatively, tunneling appears to be significant for OH + ethane-H_6 below about 250 K, for OH + methane-H_4 below about 350 K and for OH + methane-D_4 below about 225 K. In essentially all other cases it is negligible.

The primary kinetic isotope effect calculated from the six-reaction fit is compared to that calculated from the best-fit lines to the individual reaction data in Fig. 6. The 'best-fit' pKIE is shown as a thick magenta line in each case, extending only through the range of temperatures where data exist for both isotopomers. Because these individual functions fit the data with high fidelity, this magenta line can be regarded as the experimental pKIE. In all three reaction systems, the fit and the data agree to within 10% over the temperature ranges for which both hydrogen and deuterium data are available. The six-reaction fit divides the observed kinetic isotope effect between changes in the pre-factor (shown in black), the zero-point energy correction (shown in blue) and tunneling terms (shown in red) that occur upon deuteration. The pre-factor correction $\delta \ln B$ gets progressively larger as the alkanes get lighter, as shown. The zero-point energy correction remains constant across the series or reactions (as required by our model), while the changes due to tunneling become increasingly pronounced moving down the series from cyclohexane to methane. With very little deviation, the data are consistent with our model.

4. Discussion

The excellent agreement of the individual and simultaneous fit results clearly demonstrate the ability of a common set of intrinsic parameters (in a function based on the essential chemical physics controlling the rate constant) to explain the variation in rate constants within a homologous series of reactions. For the reactions considered here, these parameters are given at the top of Table 1. The co-evolution of the reaction barrier height (θ_b), the bending frequency of the radical attack (ν_1), and the tunneling temperature (θ_t) explains essentially all of the change in reactivity as the series progresses from methane to cyclohexane. The reaction-specific parameters, also listed, exert a more predictable influence over the value of the reaction rate constant, as they vary little from reaction to reaction.

The set of intrinsic parameters derived from the experimental data by the six-reaction fit are directly comparable to quantities calculated in high-level theoretical studies. Work by Melissas and Truhlar calculated the forward reaction barrier heights for the reactions of methane and ethane with OH to be 3740 and 2021 K, respectively [5,6]. Our corresponding fit values, given by $s_n\theta_b + \theta_v$, are 3379 K for methane and 2294 K for ethane. Values for the nearly degenerate ν_1 bending modes were calculated to be 316 and 357 cm^{-1} for methane, which corresponds to our fit value of 210 cm^{-1}; and 120 and 166 cm^{-1} for ethane, corresponding to our value of 120 cm^{-1}.

The behavior of two of the fit parameters is of particular interest. The first, $\delta\nu$, is the net change in vibrational frequencies on going from the reactants to the transition complex,

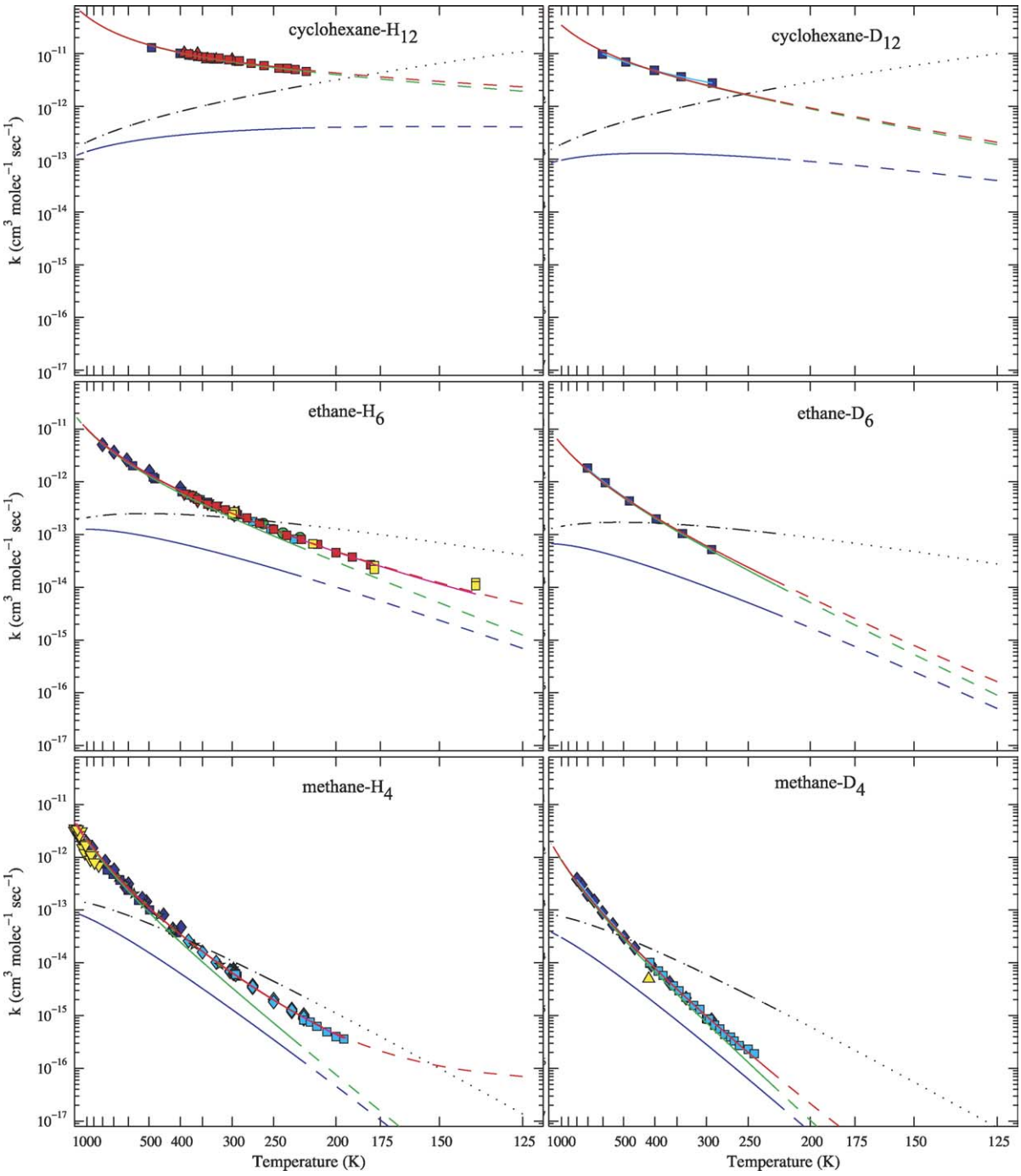

Fig. 5. Individual components of the six-reaction fit for each of the reactions. Lines are identical to those depicted in Fig. 3, though they are solid within the range of the data (for each individual reaction) and dashed outside that range. In all cases the zero-point energy correction is negative, meaning that the net effect of zero-point energy changes is to increase the barrier (the blue lines lie below the black lines). Tunneling is negligible for cyclohexane but very important for methane, while ethane is intermediate.

excluding the transition state specific modes that we model explicitly. We expect this term to be dominated by the loss of a high energy (3000 cm^{-1}) C–H stretch mode at the transition state, with small contributions, on the order of tens of wave numbers, from changes in the other vibrational modes. As such, its value in the fit was expected to remain near 3000 cm^{-1}. However, the fit consistently returned a value that was less than half of that expected, with the final six-reaction fit setting $\delta\nu = 1300\ cm^{-1}$. Fig. 6 clearly shows why. This term dominates the zero-point energy change upon deuteration (specifically, $\Delta\theta_{zp} = 1.44\delta\nu(1 - 1/\sqrt{\mu}/2)$. Our model of reactivity predicts that cyclohexane, with a low and wide barrier, should see very little tunneling, and so after correcting for $\delta \ln B$, the pKIE is due solely to $\Delta\theta_{zp}$. This value is thus tightly constrained, leaving only the relative contributions of $\delta\nu$ and μ (the reduced mass ratio). The reduced mass of C–H stretching modes is known to high accuracy, so it is very hard to imagine that this is the culprit. There is some zero-point energy along the reaction coordinate

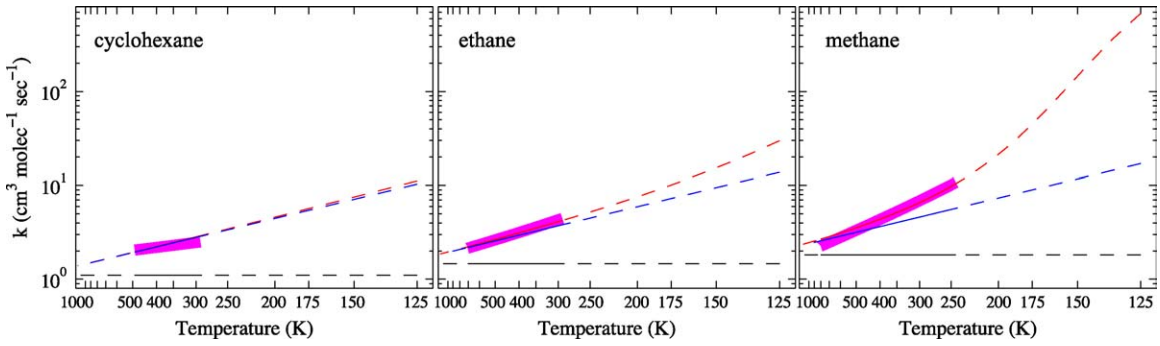

Fig. 6. Apportionment of the pKIE among its responsible terms as determined by the six-reaction fit. The contributing factors are the changes in the pre-factor (in black), the zero-point energy (in blue) and the tunneling term (in red) resulting from deuteration. The red lines also represent the six-reaction fit pKIE results; the best-fit lines to the individual reaction are shown in magenta for the temperatures for which data exist.

for H-atom transfer, as the motion is ultimately confined by the two heavy atoms (O and C), but the effective confinement is at least a factor of 3 smaller than in vibrational well of the C–H stretch, so the residual zero-point energy should be at most 10% of the original value. It is possible that the C–H bending modes are substantially stiffened at the transition state, which would counteract some of the energy loss from the C–H stretch; while we are not aware of any computational results showing a large change in the C–H bend frequencies, an underlying motivation for this work is the hypothesis that barrier frequencies are no more reliable that barrier heights in ab initio calculations.

The second interesting parameter, θ_v, is the stabilization energy of the reactants at the entrance to the reaction channel relative to their energy at far field. The six-reaction fit assigned this term a value of −930 K, indicating significant stabilization of the reactants relative to their separate energies. Before we included this term we were unable to fit the data with a common set of intrinsic parameters. Our basic model of reactivity includes a potentially strong dipole-induced dipole interaction for OH radicals [1], though it has been argued that these dipole terms are only significant for oxygen-containing organics, where hydrogen bonding can simultaneously stabilize and stiffen the transition state [26]. It is possible that this θ_v term simply represents correlation between the barrier height and key frequencies with a non-zero intercept, but it is equally likely that it is real. There is no doubt that van der Waal's complexes exist in OH + alkane systems, as they have been uneqivocally observed in molecular beam experiments [27]. The only debate is whether the complexes lie within the reaction channel. At 930 K (645 cm^{-1}) θ_v is a very modest energy, consistent with the O–H dipole being aligned parallel to the polarizable alkane electron density.

The six-reaction fit parses the available reaction energy among the several terms that control the overall rate constant, and it does so in a consistent and physically reasonable manner. For example, the rate constant for the reaction of cyclohexane with OH is 50 times faster than for the reaction of methane with OH at 1000 K, but the vibrational adiabatic rate constants for the two reactions (shown in blue in Fig. 5) are nearly identical. The only parameter in the fit that can compensate for the increasing discrepancy between the barrier and the observed rate constant at high-temperature is the term including the vibrational partition functions of the three reaction modes. As shown in Fig. 5, it does so very well by increasing for each reaction as the overall reaction barrier drops.

The parsing of energy among the various controlling factors also points to a few limitations of the six-reaction fit. In Fig. 6, the slight discrepancy between the experimental kinetic isotope effect (shown in magenta) and the result calculated from the six-reaction fit (shown in red) at the low-temperature end of the available cyclohexane data suggest that the cyclohexane fit would be better accomplished with a larger $\delta \ln B$ contribution, and an even smaller contribution from the zero-point energy difference. At the other extreme, the methane high-temperature data would be better fit with a term that made a negative contribution to the kinetic isotope effect. This discrepancy could perhaps be resolved by the inclusion of a term representing the changes in the frequencies of the 3 reaction modes upon deuteration, which is currently absent from the fit.

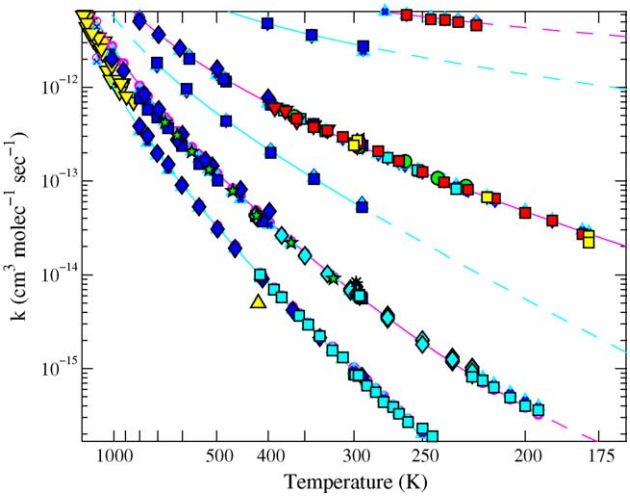

Fig. 7. Data and fit results in an Arrhenius plot for OH + methane, based on the four-reaction fit of ethane and cyclohexane (visible above the methane data). Magenta lines mark the protonated data, while cyan lines mark the deuterated data. Fits to methane-H_4 and -D_4 use parameters from ethane and cyclohexane and a single scaling factor; they are extrapolations from the faster reactions using a single free parameter.

These discrepancies notwithstanding, the simultaneous six-reaction fit reproduces the experimental data extremely well. Furthermore, because the fit is rooted in the physics of the problem it is solving, its value extends far beyond the range of the available data. The ultimate strength of the fit lies in its ability to extrapolate to temperature ranges and reaction systems for which no experimental data is available. The validity of this conjecture was tested by optimizing a four-reaction fit that excluded the methane data, and then using the intrinsic parameters from this fit to fit the methane datasets, while allowing only the scaling factor to change. The resulting fits for the methane data by this method are shown in Fig. 7. The methane data are successfully fit with the four-reaction fit parameters and a scaling factor of 1.7. In fact, the performance of this extrapolation is superb — both isotopomers of methane, when fit individually, return a scaling factor of 1.7, and, of course, the joint fit does as well. Even the quite significant curvature in the low-temperature methane-H_4 data at low temperature is reproduced, which strongly confirms that our tunneling parameterization captures real tunneling behavior quantitatively.

5. Conclusions

The method presented here incorporates multiple experimental datasets in a single non-linear least-square fit rooted in canonical transition state theory. The resulting fit accurately reproduces experimentally observed rate constants for the reaction of OH with fully hydrogenated and fully deuterated methane, ethane and cyclohexane over the entire experimentally available temperature range. Furthermore, the fit accomplishes this agreement using a common basic set of physical parameters, among which three: θ_b, θ_t and ν_1, are scaled by a simple multiplicative constant from one reaction to the next. This result supports the hypothesis that the barrier height, the barrier width and the transition state bending mode frequencies evolve in a highly correlated manner in a homologous reaction series. Additionally, the success our fit achieves by modeling the changes in reactivity along a series as a co-evolution of these three parameters provides further evidence of their common controlling physics.

Because the expression used to fit the data is based on the physics of reactivity, the parameters obtained from it are theoretically meaningful. Using these parameters, the fit can be successfully extrapolated to low temperatures where data are not available, aiding modeling efforts that require data over a broad temperature range. The development of a method similar to that presented here for systems with multiple reaction pathways (i.e. two or more types of distinguishable hydrogens) is currently underway and will generalize this approach, enabling us to further extrapolate from available experimental data toward unexplored reaction systems.

References

[1] N.M. Donahue, Reaction barriers: origin and evolution, Chem. Rev. 103 (2003) 4593.
[2] N.M. Donahue, J.G. Anderson, K.L. Demerjian, New rate constants for ten OH alkane reactions from 300 to 400 K: an assessment of accuracy, J. Phys. Chem. A 102 (1998) 3121.
[3] N.M. Donahue, Revisiting the hammond postulate: the role of reactant and product ionic state in regulating barrier heights, locations, and transition state frequencies, J. Phys. Chem. A 105 (2001) 1489.
[4] K.P. Huber, G. Herzberg, NIST Chemistry Web-Book, NIST Standard Reference Database Number 69, National Institute of Standards and Technology, Gaithersburg, MD, 20899, 2005 (Ch. Hydroxyl radical), http://webbook.nist.gov/cgi/cbook.cgi?ID=C3352576Units= SIMask= 1000Diatomic.
[5] V.S. Melissas, D.G. Truhlar, Interpolated variational transition state theory and tunneling calculation of the rate constant of the reaction $OH + CH_4$ at 223–2400 K, J. Chem. Phys. 99 (1993) 1013.
[6] V.S. Melissas, D.G. Truhlar, Interpolated variational transition state theory and semiclassical tunneling calculation of the rate constant of the reaction $OH + C_2H_6$ at 200–300 K, J. Phys. Chem. 98 (1994) 875.
[7] R.T. Skodje, D.G. Truhlar, Parabolic tunneling calculations, J. Phys. Chem. 85 (1981) 624.
[8] N.M. Donahue, J.S. Clarke, Fitting multiple datasets in kinetics: *n*-butane + OH → products, Int. J. Chem. Kinet. 36 (2004) 259.
[9] A. Bonard, V. Daele, J.-L. Delfau, C. Vovelle, Kinetics of oh radical reactions with methane in the temperature range 295–660 K and with dimethyl ether and methyl-*tert*-butyl ether in the temperature range 295–618 K, J. Phys. Chem. A 106 (2002) 4384.
[10] J.R. Dunlop, F.P. Tully, A kinetic study of OH radical reactions with methane and perdeuterated methane, J. Phys. Chem. 97 (1993) 11148.
[11] T. Gierczak, R.K. Talukdar, S.C. Herndon, G.L. Vaghjiani, A.R. Ravishankara, Rate coefficients for the reactions of hydroxyl radicals with methane and deuterated methanes, J. Phys. Chem. A 101 (1997) 3125.
[12] F.P. Tully, A.R. Ravishankara, Flash photolysis–resonance fluorescence kinetic study of the reaction $OH + H_2 \rightarrow H_2O + H$ and $OH + CH_4 \rightarrow H_2O + CH_3$, J. Phys. Chem. 84 (1980) 3126.
[13] G.L. Vaghjianai, A.R. Ravishankara, New measurement of the rate coefficient for the reaction of OH with methane, Nature 350 (1991) 406.
[14] F.P. Tully, A.T. Droege, M.L. Koszykowski, C.F. Melius, Hydrogen-atom abstraction from alkanes by OH. Part 2. Ethane, J. Phys. Chem. 90 (1986) 691.
[15] T.J. Wallington, D.M. Neuman, M.J. Kurylo, Kinetics of the gas-phase reaction of hydroxyl radicals with ethane, benzene, and a series of halogenated benzenes over the temperature range 234–438 K, Int. J. Chem. Kinet. 19 (1987) 725.
[16] J.P.D. Abbatt, K.L. Demerjian, J.G. Anderson, A new approach to free-radical kinetics: Radially and axially resolved high-pressure discharge flow with results for OH + (C_2H_6, C_3H_8, *n*-C_4H10, *n*-C_5H_{12} → products at 297 K, J. Phys. Chem. 94 (1990) 4566.
[17] A. Schiffman, J. Nelson, M.S. Robinson, D.J. Nes-bitt, High-resolution infrared flash kinetic spectroscopy of OH radicals, J. Phys. Chem. 95 (1991) 2629.
[18] R.K. Talukdar, A. Mellouki, T. Gierczak, S. Barone, S.Y. Chiang, A.R. Ravishankara, Kinetics of the reactions of OH with alkanes, Int. J. Chem. Kinet. 26 (1994) 973.
[19] J.S. Clarke, J.H. Kroll, N.M. Donahue, J.G. Anderson, Testing frontier orbital control: kinetics of OH with ethane propane, and cyclpropane from 180 to 360 K, J. Phys. Chem. A 102 (1998) 9847.
[20] P. Sharkey, I.W.M. Smith, Kinetics of elementary reactions at low-temperatures — rate constants for the reaction of OH with HCl ($298 \geq T/K \geq 138$), CH_4 ($298 \geq T/K \geq 178$) and C_2H_6 ($298 \geq T/K \geq 138$), J. Chem. Soc. Faraday Trans. 89 (1993) 631.
[21] F. Tully, A.R. Ravishankara, K. Carr, Kinetic-study of the reactions of the hydroxyl radical with ethane and propane, Int. J. Chem. Kinet. 15 (1983) 1111.
[22] D.L. Baulch, I.M. Campbell, S.M. Saunders, Rate constants for the reactions of hydroxyl radicals with propane and ethane, J. Chem. Soc. Faraday Trans. 81 (1985) 259.
[23] N.M. Donahue, J.S. Clarke, K.L. Demerjian, J.G. Anderson, Free-radical kinetics at high pressure: a mathematical analysis of the flow reactor, J. Phys. Chem. 100 (1996) 5821.

[24] N.K. Srinivasan, M.C. Su, J.W. Sutherland, J.V. Michael, Reflected shock tube studies of high-temperature rate constants for $OH + CH_4 \rightarrow CH_3 + H_2O$ and $CH_3 + NO_2 \rightarrow CH_3O + NO$, J. Phys. Chem. A 109 (2005) 1857.

[25] S. Gordon, W.A. Mulac, Reaction of the OH($X^2\Pi$) radical produced by the pulse radiolysis of water vapor, Int. J. Chem. Kinet. 7 (1975) 289.

[26] I.W.M. Smith, A.R. Ravishankara, Role of hydrogen-bonded intermediates in the bimolecular reactions of the hydroxyl radical, J. Phys. Chem. A 106 (2002) 4798.

[27] M. Tsiouris, M.D. Wheeler, M.I. Lester, Activation of the CH stretching vibrations in CH_4—OH entrance channel complexes: spectroscopy and dynamics, J. Chem. Phys. 114 (2001) 187.